How to cite: *Angew. Chem. Int. Ed.* **2020**, *59*, 18179–18183
International Edition: doi.org/10.1002/anie.202006844
German Edition: doi.org/10.1002/ange.202006844

Enantioselectivity

Near-Enantiopure Trimerization of 9-Ethynylphenanthrene on a Chiral Metal Surface

*Samuel Stolz, Aliaksandr V. Yakutovich, Jan Prinz, Thomas Dienel, Carlo A. Pignedoli, Harald Brune, Oliver Gröning, and Roland Widmer**

Abstract: *Enantioselectivity in heterogeneous catalysis strongly depends on the chirality transfer between catalyst surface and all reactants, intermediates, and the product along the reaction pathway. Herein we report the first enantioselective on-surface synthesis of molecular structures from an initial racemic mixture and without the need of enantiopure modifier molecules. The reaction consists of a trimerization via an unidentified bonding motif of prochiral 9-ethynylphenanthrene (9-EP) upon annealing to 500 K on the chiral Pd_3-terminated PdGa{111} surfaces into essentially enantiopure, homochiral 9-EP propellers. The observed behavior strongly contrasts the reaction of 9-EP on the chiral Pd_1-terminated PdGa{111} surfaces, where 9-EP monomers that are in nearly enantiopure configuration, dimerize without enantiomeric excess. Our findings demonstrate strong chiral recognition and a significant ensemble effect in the PdGa system, hence highlighting the huge potential of chiral intermetallic compounds for enantioselective synthesis and underlining the importance to control the catalytically active sites at the atomic level.*

The pronounced enantiospecific physiological effects of chiral molecules require asymmetric synthesis, for example, in pharmaceutical or food industry. Homogeneous catalysis is most widely used to obtain enantioselective synthesis via chirality transfer directly from the catalyst's organic ligand(s) despite the fact that it involves tedious separation, elaborate recycling, and its restriction to a limited temperature range.[1–3] Difficulties in separation and recycling can be alleviated by moving from homogeneous to heterogeneous catalysis.

Rational engineering of such catalysts requires fundamental understanding of the enantiospecific reactant-catalyst interaction, reaction mechanism, and kinetics. This can be achieved by investigating the interaction of molecules (educts and products) with the catalyst's surface on the atomic and molecular level and under idealized conditions, i.e., using single crystal surfaces in ultra-high vacuum (UHV).[4,5] For this purpose, achiral surfaces are commonly rendered chiral by using molecular modifiers.[6–13] This approach is marred by the need of enantiopure modifier molecules, low thermal stability, and increased complexity emerging from molecule-molecule interactions. The usage of chiral metal surfaces promises to considerably reduce complexity and increase thermal stability. Such surfaces were created by cutting achiral single crystals along low-symmetry, i.e., high Miller-index, directions.[14,15] Although the resulting surfaces exhibit only low densities of chiral centers, enantioselective decomposition of, e.g., chiral tartaric and aspartic acid was reported on Cu(643)$^{R/S}$.[16,17]

Low-index surfaces of intrinsically chiral metals offer the advantage of exhibiting orders of magnitude more chiral centers. However, today only surfaces of chiral PdGa have been sufficiently well characterized to allow the investigation of enantiospecific molecule-surface interactions, resultant molecular structures, and their formation kinetics.[18,19] Owing to its non-centrosymmetric nature,[20] PdGa exists as two enantiomorphs, PdGa:A and PdGa:B, and all its bulk truncated surfaces are chiral.[19] Here, we focus on the structurally dissimilar three-fold symmetric surfaces PdGa:A-(111)/PdGa:B($\bar{1}\bar{1}\bar{1}$) and PdGa:A($\bar{1}\bar{1}\bar{1}$)/PdGa:B(111), of which the former are terminated by single, isolated Pd atoms, referred to as Pd_1, while the latter by isolated Pd trimers, accordingly denoted Pd_3 (Figure 1a).[21] Because of this difference in combination with similar electronic properties, identical symmetry group, and the same lattice parameters,[21] PdGa{111} surfaces are ideal to disentangle the influence of geometric and electronic, i.e., ensemble and ligand, effects in enantioselective heterogeneous catalysis.[22–24]

The chirality of Pd_1 manifests itself in enantioselective adsorption at 300 K with an enantiomeric excess $ee = 100\,\% \frac{|\#R-\#S|}{\#R+\#S} = 96 \pm 2\,\%$ for prochiral 9-Ethynylphenanthrene (9-EP, Figure 1b).[25] However, no enantioselective reaction between molecules could be demonstrated on that surface.[25]

[*] Dr. S. Stolz, Dr. A. V. Yakutovich, Dr. J. Prinz, Dr. T. Dienel, Dr. C. A. Pignedoli, Dr. O. Gröning, Dr. R. Widmer
nanotech@surfaces Laboratory
Empa—Swiss Federal Laboratories for Materials Science and Technology
Überlandstrasse 129, 8600 Dübendorf (Switzerland)
E-mail: roland.widmer@empa.ch

Dr. S. Stolz, Dr. J. Prinz, Prof. Dr. H. Brune
Institute of Physics, École Polytechnique Fédérale de Lausanne
1015 Lausanne (Switzerland)

Dr. A. V. Yakutovich
Present address: Laboratory of Molecular Simulation (LSMO), Ecole Polytechnique Fédérale de Lausanne (EPFL) Valais
Rue de l'Industrie 17, 1951 Sion (Switzerland)

Dr. T. Dienel
Present address: Department of Materials Science and Engineering, Cornell University
Ithaca, NY 14853 (USA)

Supporting information (Detailed description of experimental and calculation methods, and additional STM and DFT simulations (Figures S1–S10, Table S1)) and the ORCID identification number(s) for the author(s) of this article can be found under: https://doi.org/10.1002/anie.202006844.

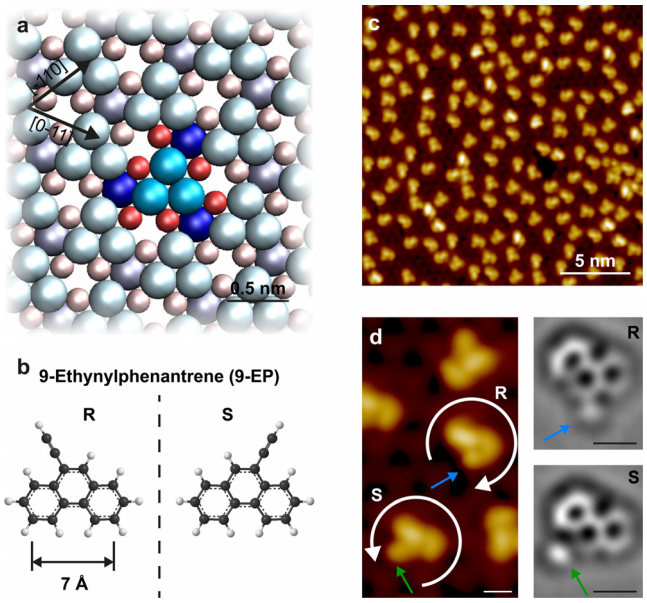

Figure 1. a) Surface structure of PdGa:A($\bar{1}\bar{1}\bar{1}$)Pd_3 with the chirality of the surface highlighted by atoms in saturated colors (that is, clearer, less washed-out colors) for one Pd trimer (top layer Pd_3 bright blue, $z=0$ nm) and its neighbors: second layer (Ga_3 red, $z=-85$ pm) and third layer (Pd_1 dark blue, $z=-161$ pm). b) molecular structure of prochiral 9-Ethynylphenanthrene (9-EP), which appears in two distinguishable surface enantiomers *R* and *S* when restricted to a planar configuration. c) STM image of 9-EP deposited at 300 K on PdGa:A($\bar{1}\bar{1}\bar{1}$)Pd_3 (bias voltage $V_B=20$ mV, tunneling current $I_T=1$ nA). d) STM image (left; $V_B=20$ mV, $I_T=10$ nA) and Gaussian-Laplace filtered nc-AFM images (right) of *R* and *S* enantiomers.

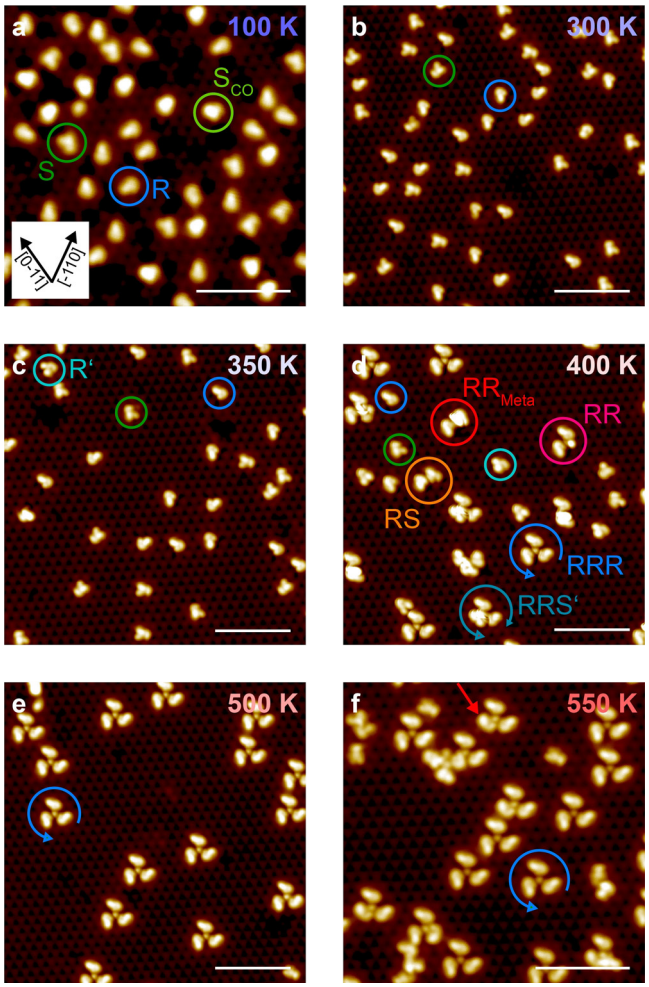

Figure 2. STM images of 9-EP on PdGa:A($\bar{1}\bar{1}\bar{1}$)Pd_3. As deposited at a) 100 K and b) 300 K. Annealing series of 9-EP on PdGa:A($\bar{1}\bar{1}\bar{1}$)Pd_3 to c) 350 K, d) 400 K, e) 500 K, and f) 550 K. STM settings: a) $V_B=50$ mV, $I_T=50$ pA; b–f) $V_B=20$ mV, $I_T=1$ nA. 9-EP/PdGa:A($\bar{1}\bar{1}\bar{1}$)Pd_3 structures are labelled according to the nomenclature in the text. The red arrow in (f) indicates an exemplary 9-EP integrated in a trimer with disintegrated alkyne group. All scale bars correspond to 5 nm.

Here, we study the near-enantiopure trimerization from an initial racemic mixture of 9-EP on PdGa:A($\bar{1}\bar{1}\bar{1}$)Pd_3 (A:Pd_3) by scanning tunneling microscopy (STM), CO-sensitized non-contact atomic force microscopy (nc-AFM), and density functional theory (DFT) calculations.

Deposition of sub-monolayer coverages of 9-EP onto the A:Pd_3 surface kept at 300 K results in a homogeneous coverage of well isolated molecules when imaged at 5 K (Figure 1c). Analysis of adsorption site and molecule orientation reveals that the vast majority of 9-EP are present in two disparate configurations, each appearing in three symmetrically equivalent geometries. Combining high-resolution STM and nc-AFM images, the nature of these two distinct 9-EP configurations can be assigned to its *R* and *S* surface enantiomorphs (Figure 1d). The STM signature of the *S* configuration is an elongated protrusion (green arrows in Figure 1d) attributed to the alkyne group pointing towards the right of the phenanthrene backbone. Conversely, the adsorption configuration of the *R* surface-enantiomer leads to a dot like imaging of the alkyne group (blue arrows in Figure 1d).

Deposition at 100 K and 300 K substrate temperature results in basically identical adsorption configurations, as evidenced in Figures 2a,b. In both cases, the adsorbates are *R* and *S* enantiomers with equal abundance (100 K: $ee=4\pm5\%$; 300 K: $ee=4\pm4\%$). In some cases, *S* enantiomers seem to have some co-adsorbate, most likely CO, attached (labelled S_{CO}). Upon annealing to 350 K an $ee=19\pm5\%$ in favor of *R* evolves (Figure 2c). We therefore conclude that (i) the energy barrier for *S* to *R* interconversion can be overcome above 300 K, and (ii) *R* 9-EP is energetically preferred over *S* 9-EP on A:Pd_3. Concomitantly, the occurrence of S_{CO} is reduced to virtually zero due to CO desorption,[26] and a new species labelled *R'* (Figure 3b), representing the same surface enantiomorph as *R* but being adsorbed on a different site, emerges in low numbers.

We attribute the moderate *R* enantiomeric excess on A:Pd_3 to dissimilar lattice sites of the *R* and *S* alkyne groups, resulting in slight adsorption energy differences. Whereas the alkyne group peripherally overlaps with one Pd atom of the substrate trimer for *R*, it completely covers the Pd trimer for *S*. The phenanthrene backbone exhibits in both cases an identical adsorption configuration (Figure 3a). This difference in adsorption geometry will become decisive in the formation of chiral 9-EP oligomers, as we will show in the following.

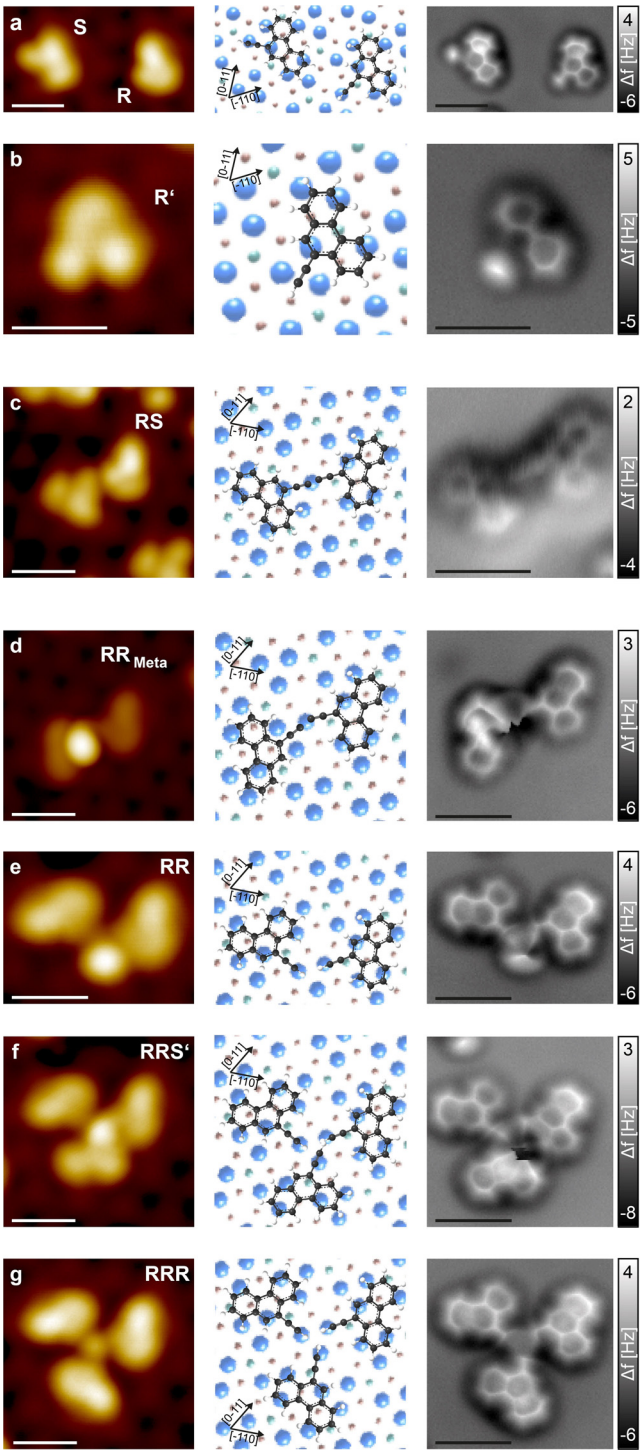

Figure 3. STM image (left) with the adsorption configuration determined by overlaying the STM images with the atomic surface structure (center) and the corresponding nc-AFM images (right) for (a) *R*, *S* and (b) *R*′ monomer, the (c) *RS*, (d) RR_{Meta} and (e) *RR* dimer, and the (f) *RRS*′ and (g) *RRR* trimers. STM settings a),b),d)–g) $V_B = 50$ mV, $I_T = 10$ pA; c) $V_B = 20$ mV, $I_T = 2$ nA. All scale bars represent 1 nm.

Upon annealing at 400 K, 9-EP dimers and trimers are forming (Figure 2d), of which 92% exhibit well-defined configurations that can be classified into the 5 species shown in Figures 3c–g. We will refer to 9-EP trimers as propellers based on their appearance. A common feature of all 9-EP oligomers is that they are linked with their alkyne group positioned on the same Pd trimer, facing each other. Additionally, several peculiarities related to the participation of *R* and *S* enantiomers in the oligomers are recognized. First, the *R* enantiomers in all coupled structures are on identical adsorption sites as the isolated *R* (except for one 9-EP contained in the RR_{Meta} dimer in Figure 3d). Second, *S*′ in a propeller exhibits a different positional and orientational configuration as the isolated *S*. Third, the entire absence of homochiral *S* or *S*′ dimers and propellers. Without enantioselectivity, one expects a statistical propeller occurrence of $RRR{:}RRS'{:}RS'S'{:}S'S'S' = {}^1/_8 : {}^3/_8 : {}^3/_8 : {}^1/_8$. Instead, we observe relative abundancies of $^6/_8 : {}^2/_8 : {}^1/_{100} : 0$ (459 monomer units analyzed). This implies a strong bias towards the incorporation of *R* 9-EP in propellers, the probability amounts to roughly 90%, and yields an RRR enantiomeric excess of $ee_{RRR} = 100\,\% \frac{\#RRR - \#RRS' - \#RS'S' - \#S'S'S'}{\#RRR + \#RRS' + \#RS'S' + \#S'S'S'} = 49 \pm 4\,\%$ at 400 K.

Increasing the annealing temperature to 500 K (Figure 2e) raises the yield of propellers from around 50% to more than 86% with a corresponding decrease of dimers and monomers. The full temperature dependent development of 9-EP structures and their relative coverage, i.e., the species' coverages normalized to the overall number of 9-EP units, is summarized in Figure 4. Besides propellers becoming the most abundant species at 500 K, they also evolve into homochiral, enantiopure RRR propellers (Figure 4b) with ee_{RRR} rising to staggering 97% ±2%, which corresponds to a 99.5% probability of a 9-EP in the propeller being in form *R*. Moreover, *RR* and RR_{Meta} vanish at 500 K and only *RS* along with various other unidentified dimer structures with a collective yield of 6% remain.

Annealing to 550 K initiates decomposition of 9-EP, presumably at the alkyl group, as evident from the emergence of propellers with one 9-EP unit closer to the connecting center (Figure 2f). Therefore, temperatures beyond 500 K have not been considered in our analysis.

Among all 9-EP oligomers, the structural identification of *RS* dimers presented in Figure 3c is most straightforward. Their *R* and *S* elements must be dehydrogenatively covalently coupled because pristine *R* and *S* enantiomers cannot be present in such close proximity due to steric hindrance of their alkyne groups. Our interpretation is supported by the bond distances inferred from nc-AFM and their persistence upon annealing to 500 K (Figure 4b). This stability contrasts to that of the *RR* and RR_{Meta} dimers (Figures 3d,e), which are present at 400 K but vanish upon annealing to 500 K (Figure 4b). The depletion of *RR* and RR_{Meta} dimers suggests them to be precursors for 9-EP propellers (Figure S5). Both dimers are characterized by an apparent connection at the alkyne groups. This connection site shows up as bright protrusion in the STM images (bias dependent), indicating an extended connecting moiety, which, however, cannot be resolved by nc-AFM.

While *RRS*′ exhibits a similarly strong protrusion in STM images as *RR* and RR_{Meta} dimers, the protrusion of *RRR*

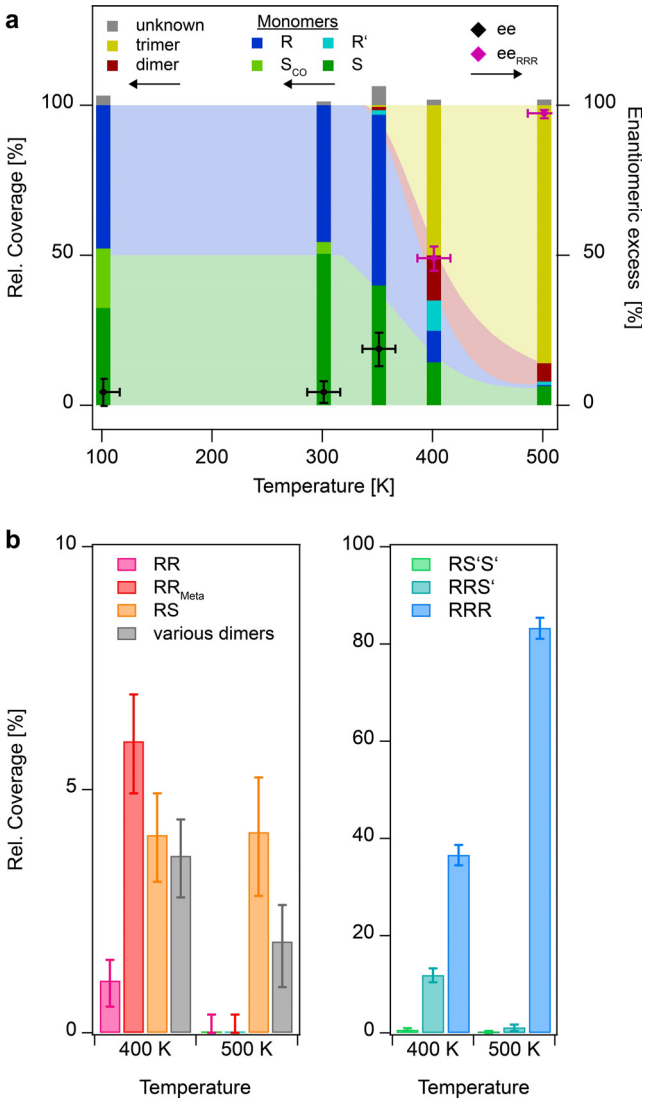

Figure 4. a) Color map of the relative coverage of 9-EP monomers, dimers, and trimers together with the enantiomeric excess as function of adsorption/annealing temperature on PdGa:A($\bar{1}\bar{1}\bar{1}$)Pd_3. b) Relative coverage of various 9-EP dimers (left) and trimers (right) at annealing temperatures 400 K and 500 K.

propellers is a less-pronounced, well-defined central dot (Figure 3 f,g; for detailed STM characterization of *RRR* propellers, see Figure S3,S4). The corresponding nc-AFM image of *RRR* (Figure 3 g) is featureless in the center, but displays its *R* elements alike individual *R* monomers (Figure 3 a). The near-complete absence of *RRS′* at 500 K implies that this species, alike *RR* and RR_{Meta} dimers, is a metastable precursor of RRR propellers. The conversion of *RRS′* into *RRR* requires the wrong-handed *S′* incorporated into a propeller to convert into the R configuration.

So far, only the dehydrogenative covalent coupling of *RS* dimers could be unambiguously deduced. Identification of the *RR*, RR_{Meta} and *RRS′* coupling is hampered by their presumably non-planar motif observed in nc-AFM (Figures 3 d–f). For RRR, the central link exhibits a surprisingly featureless nc-AFM signature (Figure 3 g), preventing elucidation of its atomic structure.

As 9-EP on A:Pd_3 is mobile at 300 K (Figure S6), the oligomers cannot be unspecifically bonded entities held together by weak interactions (e.g., electrostatic), which is corroborated by the low energy gain derived from DFT (Table S1). We rather postulate an activated oligomerization via strong bond formation which is supported by the fact that the trimers are impossible to separate by STM-tip induced manipulation. The likeliest mechanisms are either a [2+2+2] cyclization of alkynes, which has been reported for different molecules on Au(111)[27–29] and Cu(111),[30] or a coordination to individual Pd or Ga surface adatoms or to carbon-based fragments. The [2+2+2] cyclization as formation mechanism of the 9-EP propellers can be excluded due to the excessively large spatial separation of the phenanthrene moieties (Figure S7). Also the coordination of 9-EP molecules to Pd or Ga adatoms has to be discarded as direct evaporation of the respective metals does not aid the expected oligomer formation (Figures S8,S9). Neither does benzene stabilize the oligomers as benzene desorbs below 350 K, just like other small carbon-based molecules such as acetylene, ethylene, and CO,[26,31] nor deliver simulated nc-AFM images of 9-EP coupled via additional central carbon species signatures comparable to the experimental ones (Figure S10). Therefore, the bonding motif of the 9-EP molecules building homochiral and highly enantioselective 9-EP propellers remains unresolved and thus limits our discussion of their synthesis to experimental observations.

We have presented a detailed study of the first asymmetric heterogeneous coupling reaction on an intrinsically chiral metal surface, which requires no enantiopure precursor or modifier molecules. Specifically, we investigated the oligomerization of 9-EP on PdGa:A($\bar{1}\bar{1}\bar{1}$)Pd_3. The adsorption of 9-EP monomers as *R* and *S* enantiomorphs is governed by the identical configuration of the phenanthrene moiety and the energetic difference only resides in the interaction of the alkyne group with the substrate. This minor difference in the 9-EP adsorption configuration between *R* and *S* seems to be the origin of the enantioselective formation of homochiral 9-EP trimers at 500 K with an enantiomeric excess of 97 % because the adsorption configuration of each 9-EP unit in the *RRR* trimer remains exactly the same as for an isolated *R* monomer.

Owing to the ensemble effect, the temperature evolution of the enantiomeric excess of 9-EP structures and reaction products on PdGa{111}Pd_3 are in stark contrast to those on PdGa{111}Pd_1.[25] Specifically, whereas on PdGa{111}Pd_3, 9-EP monomers occur in a racemic mixture at 300 K, they appear with an enantiomeric excess of 96 % on PdGa{111}Pd_1 due to a lower energy barrier for the conversion between *R* and *S* monomers and the enantiospecific van der Waals interaction with the substrate's second layer Ga trimer.[32] At elevated temperatures, however, all 9-EP molecules form stable dimers on PdGa{111}{Pd_1 without enantioselectivity, whereas dimers on PdGa{111}Pd_3 are metastable and primarily intermediates for the homochiral and virtually enantiopure trimerization.

The obvious disparities in reaction pathway, kinetics, and enantioselectivity for the two structurally different PdGa{111} surfaces underline the significance of the ensemble effect and the need for an understanding of molecule-substrate interaction at atomic scales. Moreover, the reported creation of near-enantiopure molecular structures from a racemic mixture of precursor constitutes a significant advancement towards enantioselective heterogeneous catalysis on chiral metallic surfaces.

Acknowledgements

We acknowledge funding from the Swiss National Science Foundation under SNSF project number 159690. T.D. acknowledges support by NSF-Platform for the Accelerated Realization, Analysis and Discovery of Interface Materials (PARADIM, DMR-1539918).

Conflict of interest

The authors declare no conflict of interest.

Keywords: asymmetric catalysis · chirality · enantioselectivity · intermetallic compounds · scanning probe microscopy

[1] M. Heitbaum, F. Glorius, I. Escher, *Angew. Chem. Int. Ed.* **2006**, *45*, 4732 – 4762; *Angew. Chem.* **2006**, *118*, 4850 – 4881.
[2] G. Kyriakou, S. K. Beaumont, R. M. Lambert, *Langmuir* **2011**, *27*, 9687 – 9695.
[3] S. Bellemin-Laponnaz, T. Achard, D. Bissessar, Y. Geiger, A. Maisse-François, *Coord. Chem. Rev.* **2017**, *332*, 38 – 47.
[4] G. A. Somorjai, *Science* **1985**, *227*, 902 – 908.
[5] G. Ertl, H.-J. Freund, *Phys. Today* **1999**, *52*, 32 – 38.
[6] F. Zaera, *Chem. Soc. Rev.* **2017**, *46*, 7374 – 7398.
[7] S. Dutta, A. J. Gellman, *Chem. Soc. Rev.* **2017**, *46*, 7787 – 7839.
[8] D. Stacchiola, L. Burkholder, W. T. Tysoe, *J. Am. Chem. Soc.* **2002**, *124*, 8984 – 8989.
[9] M. Parschau, S. Romer, K.-H. Ernst, *J. Am. Chem. Soc.* **2004**, *126*, 15398 – 15399.
[10] F. Gao, Y. Wang, Z. Li, O. Furlong, W. T. Tysoe, *J. Phys. Chem. C* **2008**, *112*, 3362 – 3372.
[11] I. Lee, F. Zaera, *J. Am. Chem. Soc.* **2006**, *128*, 8890 – 8898.
[12] D. J. Watson, R. J. Bennie Ram John Jesudason, S. K. Beaumont, G. Kyriakou, J. W. Burton, R. M. Lambert, *J. Am. Chem. Soc.* **2009**, *131*, 14584 – 14589.
[13] T. J. Lawton, V. Pushkarev, D. Wei, F. R. Lucci, D. S. Sholl, A. J. Gellman, E. C. H. Sykes, *J. Phys. Chem. C* **2013**, *117*, 22290 – 22297.
[14] C. F. McFadden, P. F. Cremer, A. J. Gellman, *Langmuir* **1996**, *12*, 2483 – 2487.
[15] D. S. Sholl, A. J. Gellman, *AIChE J.* **2009**, *55*, 2484 – 2490.
[16] A. J. Gellman, Y. Huang, X. Feng, V. V. Pushkarev, B. Holsclaw, B. S. Mhatre, *J. Am. Chem. Soc.* **2013**, *135*, 19208 – 19214.
[17] B. S. Mhatre, S. Dutta, A. Reinicker, B. Karagoz, A. J. Gellman, *Chem. Commun.* **2016**, *52*, 14125 – 14128.
[18] M. Armbrüster, K. Kovnir, M. Behrens, D. Teschner, Y. Grin, R. Schlögl, *J. Am. Chem. Soc.* **2010**, *132*, 14745 – 14747.
[19] D. Rosenthal, R. Widmer, R. Wagner, P. Gille, M. Armbrüster, Y. Grin, R. Schlögl, O. Gröning, *Langmuir* **2012**, *28*, 6848 – 6856.
[20] M. Armbrüster, H. Borrmann, M. Wedel, Y. Prots, R. Giedigkeit, P. Gille, *Z. Kristallogr. New Cryst. Struct.* **2010**, *225*, 617 – 618.
[21] J. Prinz, R. Gaspari, C. A. Pignedoli, J. Vogt, P. Gille, M. Armbrüster, H. Brune, O. Gröning, D. Passerone, R. Widmer, *Angew. Chem. Int. Ed.* **2012**, *51*, 9339 – 9343; *Angew. Chem.* **2012**, *124*, 9473 – 9477.
[22] W. M. H. Sachtler, *Catal. Rev. Sci. Eng.* **1976**, *14*, 193 – 210.
[23] P. Liu, J. K. Nørskov, *Phys. Chem. Chem. Phys.* **2001**, *3*, 3814 – 3818.
[24] J. K. Nørskov, T. Bligaard, B. Hvolbæk, F. Abild-Pedersen, I. Chorkendorff, C. H. Christensen, *Chem. Soc. Rev.* **2008**, *37*, 2163 – 2171.
[25] J. Prinz, O. Gröning, H. Brune, R. Widmer, *Angew. Chem. Int. Ed.* **2015**, *54*, 3902 – 3906; *Angew. Chem.* **2015**, *127*, 3974 – 3978.
[26] J. Prinz, R. Gaspari, Q. S. Stöckl, P. Gille, M. Armbrüster, H. Brune, O. Gröning, C. A. Pignedoli, D. Passerone, R. Widmer, *J. Phys. Chem. C* **2014**, *118*, 12260 – 12265.
[27] H. Zhou, J. Liu, S. Du, L. Zhang, G. Li, Y. Zhang, B. Z. Tang, H.-J. Gao, *J. Am. Chem. Soc.* **2014**, *136*, 5567 – 5570.
[28] J. Liu, P. Ruffieux, X. Feng, K. Müllen, R. Fasel, *Chem. Commun.* **2014**, *50*, 11200.
[29] F. Xiang, Y. Lu, C. Li, X. Song, X. Liu, Z. Wang, J. Liu, M. Dong, L. Wang, *Chem. Eur. J.* **2015**, *21*, 12978 – 12983.
[30] J. Eichhorn, W. M. Heckl, M. Lackinger, *Chem. Commun.* **2013**, *49*, 2900.
[31] J. Prinz, C. A. Pignedoli, Q. S. Stöckl, M. Armbrüster, H. Brune, O. Gröning, R. Widmer, D. Passerone, *J. Am. Chem. Soc.* **2014**, *136*, 11792 – 11798.
[32] A. V. Yakutovich, J. Hoja, D. Passerone, A. Tkatchenko, C. A. Pignedoli, *J. Am. Chem. Soc.* **2018**, *140*, 1401 – 1408.

Manuscript received: May 12, 2020
Accepted manuscript online: June 26, 2020
Version of record online: August 13, 2020

